JGR Solid Earth

RESEARCH ARTICLE
10.1029/2025JB031123

Paleomagnetic Evidence for a Late Permian Qaidam-North China Connection, and the Cryptic Final Mesozoic Intra-Asian Suture

Teng Wang[1,2], Yanan Zhou[1], Douwe J. J. van Hinsbergen[2], Jiaopeng Sun[1], Xin Cheng[1], Ruiyang Chai[1], Shihua Xu[2,3], Pengfei Wang[1], and Hanning Wu[1]

[1]State Key Laboratory of Continental Evolution and Early Life, Department of Geology, Northwest University, Xi'an, China, [2]Department of Earth Sciences, Utrecht University, Utrecht, Netherlands, [3]State Key Laboratory for Mineral Deposits Research, School of Earth Sciences and Engineering, Institute of Continental Geodynamics, Nanjing University, Nanjing, China

Abstract Paleomagnetic data have long shown that the final assembly of eastern Eurasia occurred in the latest Jurassic, after the North China Block moved 1,000 s of km toward Eurasia throughout the late Paleozoic and Mesozoic. This was accommodated along the Solonker and Mongol-Okhotsk subduction zones whose sutures are well documented in (inner) Mongolia. During this time, one or more plate boundaries must have existed west of China to connect the (inner) Mongolian suture with the Paleotethyan plate boundaries. Paradoxically, no candidate Mesozoic plate boundary is known between North China and Eurasia to its west, in northern Tibet, the Tarim Basin, or the Tien Shan region. In this study, we show paleomagnetic pole from Upper Permian (255.7 ± 3.8 Ma) red beds from the Qaidam Block of northern Tibet, adjacent to the Tarim Basin, with positive fold test and corrected for inclination shallowing, with $D = 348.7° \pm 2.3°$, $I = 47° \pm 2.5°$, $\lambda = 77.6°$N, $\phi = 332.8°$E, $A_{95} = 2.1°$, $K = 24.7$, $N = 199$. These data reveal that Qaidam Block's paleolatitude was indistinguishable from that expected if it was part of North China but must have undergone ~21° ± 2° (>2,300 ± 220 km) paleolatitudinal motion relative to Eurasia since late Permian time. This suggests that the missing plate boundary (or boundaries), in the form of a transform or a subduction zone, must be sought around or within the Tarim Basin. This may form a starting point in a search for the cryptic, last intra-Asian suture(s) and calls for systematic regional restoration of circum-Tarim tectonic history.

Plain Language Summary Previous studies found that the distance between the North China Block and Eurasia was more than 2,000 km in late Permian time, and its northward motion relative to Eurasia occurred until the latest Jurassic closure of the Mongol-Okhotsk suture. Where this plate motion was accommodated to the west of North China, around the Tarim Basin and the northern Tibetan Plateau, however, is unknown. In this study, we obtain a paleomagnetic result from Upper Permian red beds in the Qaidam Block of northeast Tibet, which is located between the North China Block and Tarim Basin, and show that the Qaidam Block underwent the same post-late Permian paleolatitudinal motion as North China Block. This shows that a cryptic former plate boundary between the plates that carried North China and Eurasia must be located at the boundaries of, or within the Tarim Basin, which provides a starting point for targeted mapping and reconstruction of the last major plate boundary that formed the Eurasian continent.

Key Points:

- Paleomagnetic results obtained from Upper Permian red beds from the Qaidam Block show paleolatitudinal separation from Eurasia of ~21°
- The Qaidam and North China Blocks underwent the same post-late Permian paleolatitudinal motions and were likely connected
- A cryptic Mesozoic plate boundary is required between Qaidam and Eurasia, likely below the Tarim basin

Supporting Information:

Supporting Information may be found in the online version of this article.

Correspondence to:

Y. Zhou,
zhouyanan@nwu.edu.cn

Citation:

Wang, T., Zhou, Y., van Hinsbergen, D. J. J., Sun, J., Cheng, X., Chai, R., et al. (2025). Paleomagnetic evidence for a late Permian Qaidam-North China connection, and the cryptic final Mesozoic intra-Asian suture. *Journal of Geophysical Research: Solid Earth*, *130*, e2025JB031123. https://doi.org/10.1029/2025JB031123

Received 15 JAN 2025
Accepted 30 JUL 2025

Author Contributions:

Conceptualization: Teng Wang, Douwe J. J. van Hinsbergen
Data curation: Teng Wang, Shihua Xu
Funding acquisition: Yanan Zhou, Hanning Wu
Investigation: Teng Wang, Yanan Zhou, Jiaopeng Sun, Xin Cheng, Ruiyang Chai, Pengfei Wang
Writing – original draft: Teng Wang, Yanan Zhou
Writing – review & editing: Douwe J. J. van Hinsbergen

1. Introduction

The modern continents typically consist of older continental fragments with Precambrian basement cores and sedimentary covers, separated by suture zones and associated accretionary orogens (Cawood et al., 2009; Xiao et al., 2015). Such suture zones are straightforwardly recognized if relics of subducted oceanic crust are still present in the geological record as accreted oceanic volcanic and sedimentary rocks (Cawood et al., 2009; Isozaki et al., 1990). However, if oceanic lithosphere subducts without accretion, or when accretionary relics are obscured by younger sedimentary covers or orogens, or were dominated by transform motion, the locations of former plate boundaries may be challenging to identify, and the geological record may become difficult to reconcile with plate kinematic reconstructions (van Hinsbergen, 2022). The closure of the last major ocean during the assembly of the eastern Eurasian continent, which culminated in the accretion of the China blocks, is in places associated with such a cryptic Mesozoic paleo-plate boundary.

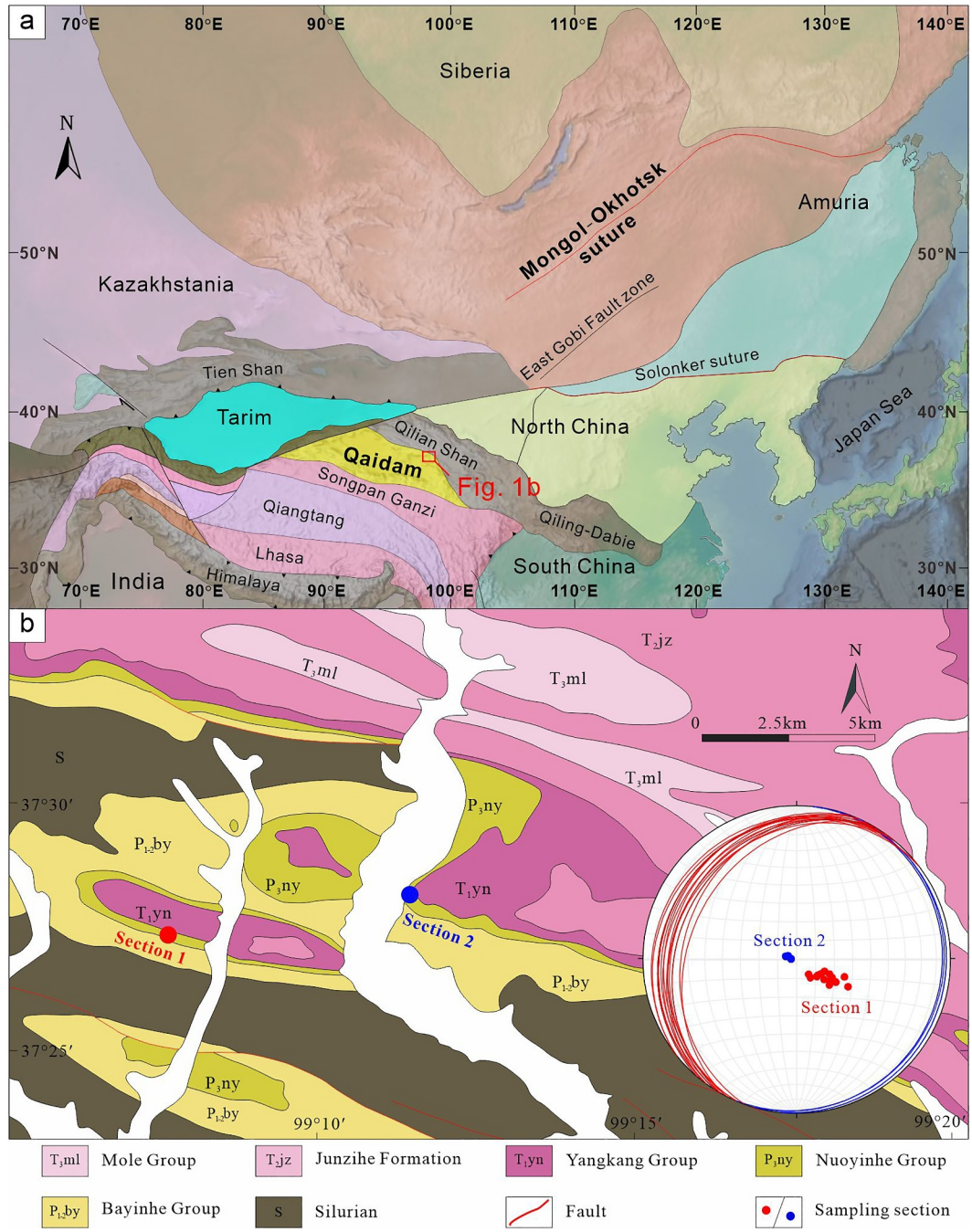

Figure 1. Geological map of the study area. (a) Simplified tectonic map of Asia showing the main boundaries in this paper (modified from Van der Voo et al., 2015; van Hinsbergen et al., 2011). (b) Geological map of the sampling locations in the Tianjun area (QBGMR, 1976) and the lower hemisphere stereonet projection for the bedding attitudes of the Nuoyinhe Group red beds.

The eastern Eurasian continent contains several major continental fragments (Figure 1a) that accreted to the Siberian Craton over time. These include the North China Block and the Tarim Block, and a major accretionary orogen known as the Central Asian Orogenic belt derived from subducted oceanic and microcontinental lithosphere (e.g., Eizenhöfer et al., 2014; Şengör et al., 1993; D. Song et al., 2018; Van der Voo et al., 2015; Xiao et al., 2015, 2020; Zhao et al., 2018). The Mongol-Okhotsk suture in Mongolia and far-eastern Russia is the youngest suture to form between the North China Block and Eurasia and contains evidence for a latest Jurassic

age of ocean closure (e.g., Jolivet et al., 2017; T. Wang et al., 2022). This is fully consistent with paleomagnetic evidence from the North China Block that shows significant paleolatitudinal convergence with Siberia until the latest Jurassic-early Cretaceous (Cogné et al., 2005; Van der Voo et al., 2015). Paradoxically, the youngest known suture between the North China Block and Eurasia to the west, located in the Tien Shan mountains between the Tarim Block and Eurasia, is Permian in age (e.g., Allen et al., 1993; Xiao et al., 2013, 2020).

Plate-kinematic logic requires that a plate carrying the North China Block was separated by a plate boundary from Eurasia to the north until latest Jurassic time, a plate boundary should also have existed between North China and Eurasia in the west, and this ending in a triple junction with the Tethyan sutures in the south (Van der Meer et al., 2018; Van der Voo et al., 2015). However, the absence of a clearly defined suture between the North China and Tarim Blocks is puzzling and reconstructing the final amalgamation of east Asia is therefore challenging. If a Mesozoic plate boundary existed here, it must have been buried, tectonically or by sediments.

The Qaidam Block of northern Tibet is separated from the Tarim Block and the North China Block by major Cenozoic fault zones that could perhaps hide a cryptic Mesozoic plate boundary (Figure 1a). To the west, it is separated by the major Altyn Tagh fault from the Tarim Basin (Sobel & Arnaud, 1999). To the east it is separated by the Qilian Shan fold-thrust belt from North China (Yin & Harrison, 2000). Here, we present new paleomagnetic data from upper Permian sedimentary rocks in the Qaidam Block to evaluate whether the basin moved together with the North China Block or with the Tarim Basin/Eurasia, or neither, since latest Paleozoic time. We will use our results to evaluate where the latest Paleozoic-early to mid-Mesozoic North China-Eurasia plate boundary, connecting the (inner) Mongolian and Tethyan suture zones may be sought.

2. Geological Setting and Sampling

Our study area is in folded and thrusted portions of the northeastern part of the Qaidam Block, in the north of Tianjun County, where Paleozoic to Cenozoic strata are widely exposed. Sediments in the selected time interval, in the Permian, were deposited in a non-marine to shallow-marine environment in the upper plate of a Paleo-tethyan subduction system that is marked by the Kunlun Arc, just to the south of the Qaidam Block (Dong et al., 2018; Kapp & DeCelles, 2019; Yin & Harrison, 2000). We collected rocks from the Upper Permian Nuoyinhe Group (Figure 1b), which is mainly composed of thick-layered muddy siltstones interbedded with limestones in the lower part, and grading into purple-red sandstones in the upper part (Figure 2 and Figure S1 in Supporting Information S1). The Nuoyinhe Group is dated at Lopingian (259.5–251.9 Ma) through brachiopods (including *Waagenites* cf., *Leptodus nobilis*, *Megaderbyia magnifica*, *Buxtonia costatoconcentrica*, *Composita yangkangensis*), and bivalves (including *Myalinella* sp.) (Liu, 1980; Lu, 1986; QBGMR, 1976). To verify the deposition age of Nuoyinhe Group, we collected a sandstone sample (23TJG01) (37.45°N/99.06°E) for detrital zircon U-Pb dating to constrain the maximum depositional age.

Previously, Xu et al. (2011) reported paleomagnetic results from the Nuoyinhe Group. Their study involved a total of nine sampling locations from which a total of 56 samples were collected that predicted a low paleolatitude for their sampling location of ∼24°N, where a paleolatitude of ∼49° would have been expected for Eurasia (Vaes et al., 2023). The low amount of data from this study did not permit inclination shallowing correction, as the E/I method that corrects this bias requires a minimum of ∼80 samples (Tauxe & Kent, 2004; Vaes et al., 2021). As a result, the paleolatitude estimate of Xu et al. (2011) is probably too low.

For our study, we collected a total of 240 cores from 25 sampling locations divided over two sections within the Nuoyinhe Formation with different bedding attitude, to allow for fold test. Sample were collected by drilling across the stratigraphy, so that each core may be regarded as a spot reading of the magnetic field, so that the data set may be compared with the expected distribution of paleomagnetic data as a result of paleosecular variation (PSV) of the paleomagnetic field—the basic assumption underlying the *E/I* method (Tauxe & Kent, 2004; Vaes et al., 2021). For sampling, we used a hand-held gasoline-powered motor drill. A total of 173 samples were collected from Section 1 (37.47°N/99.14°E) located in the north of Tianjun County, and 67 samples were obtained from seven sampling locations from Section 2 located in the northeast of Tianjun County (37.45°N/99.06°E), ∼10 km to the east (Figure 1b).

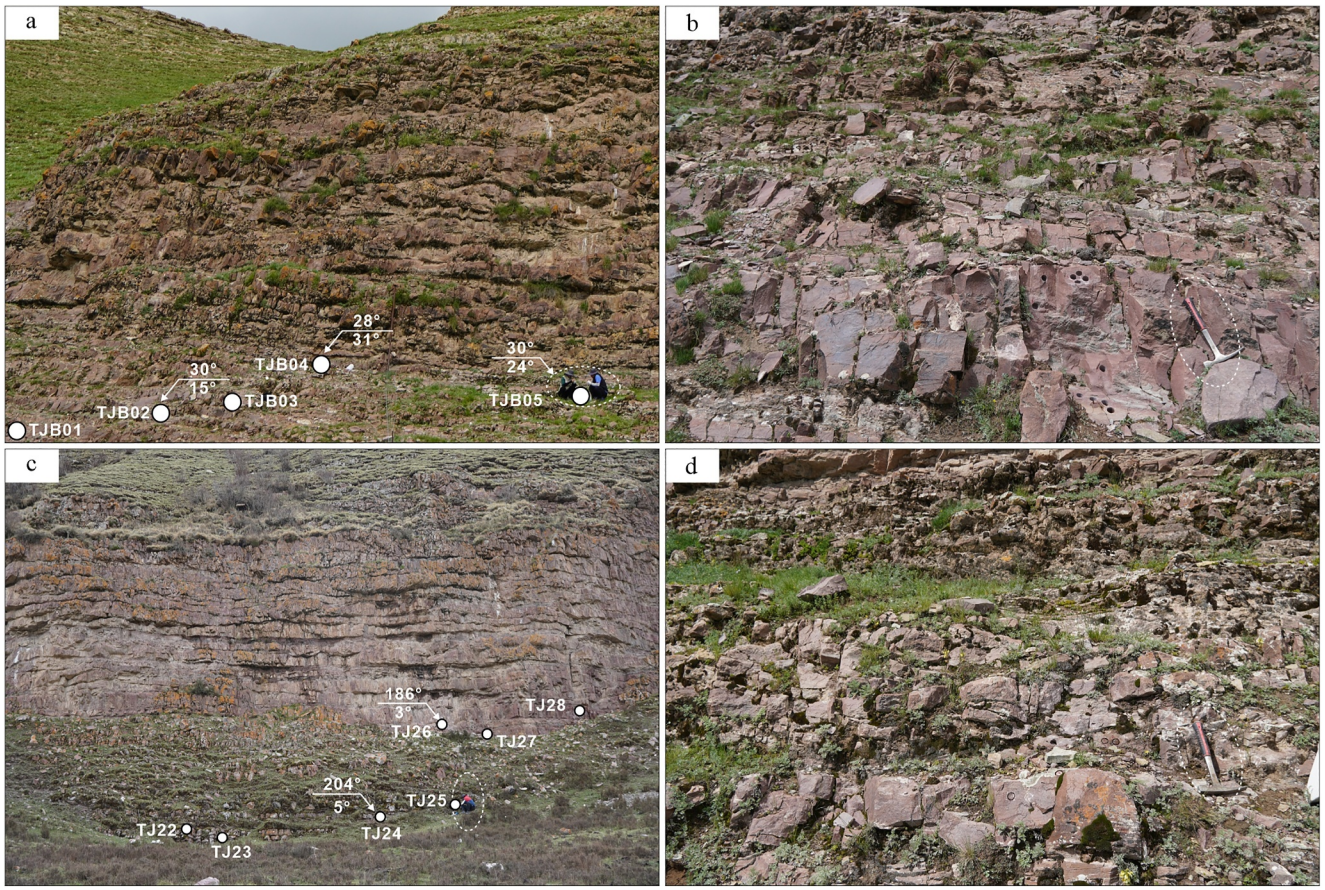

Figure 2. Representative field photographs of sampling outcrops. (a, b) Red beds of Nuoyinhe Formation from Section 1; (c, d) Red beds of Nuoyinhe Formation from Section 2. The geologist in Figures 3a and 3c is approximately 175 cm tall; the geological hammer in Figures 3b and 3d is 35 cm in length.

3. Methods

For detrital zircon geochronology, zircon grains were separated magnetically, using heavy liquids, and finally hand-picked under a binocular microscope at the Langfang Regional Geological Survey in China. The zircons were mounted in epoxy resin blocks and polished to flat surfaces. Cathodoluminescence images and U-Pb dating were conducted at the State Key Laboratory of Continental Dynamics, Northwest University (Xi'an, China). Methods for Laser Ablation Inductively Coupled Plasma Mass Spectrometry (LA-ICP-MS) zircon U-Pb dating are detailed in T. Wang et al. (2023) and references therein. Concordia ages were calculated with the Isoplot (3.0) (Ludwig, 2003).

Each oriented paleomagnetic core was cut into 1–2 specimens of 2.2 cm in length. Rock magnetic, thermal demagnetization and remanent magnetizations measurement experiments were completed in the Paleomagnetic Laboratory of Northwest University (Xi'an, China). Field samples were oriented in situ using both magnetic compass and solar compass when weather permitted. The declination difference observed between these two orientation methods is less than 2°, showing that local magnetic disturbances in the sampled area are insignificant.

Isothermal remanent magnetization (IRM) acquisition experiments, reverse field demagnetization experiments and thermal demagnetization of three-component IRMs were performed with an ASC IM-10-30 pulse magnetizer, JR-6A magnetometer, and TD-48 thermal demagnetization furnace, respectively. Magnetic susceptibility versus temperature (*k*-T) experiments were conducted in air using an MFK2 Susceptibility meter with CS-4 temperature control system. Anisotropy of magnetic susceptibility (AMS) measurements were carried out using an AGICO Kappabridge KLY-4S susceptibility meter. Scanning electron microscope (SEM) and energy dispersive spectrometer (EDS) were carried out using FEI Quanta 400 FEG 20 kV and an OXFORD IE 350 at the State Key Laboratory of Continental Dynamics, Northwest University (Xi'an, China).

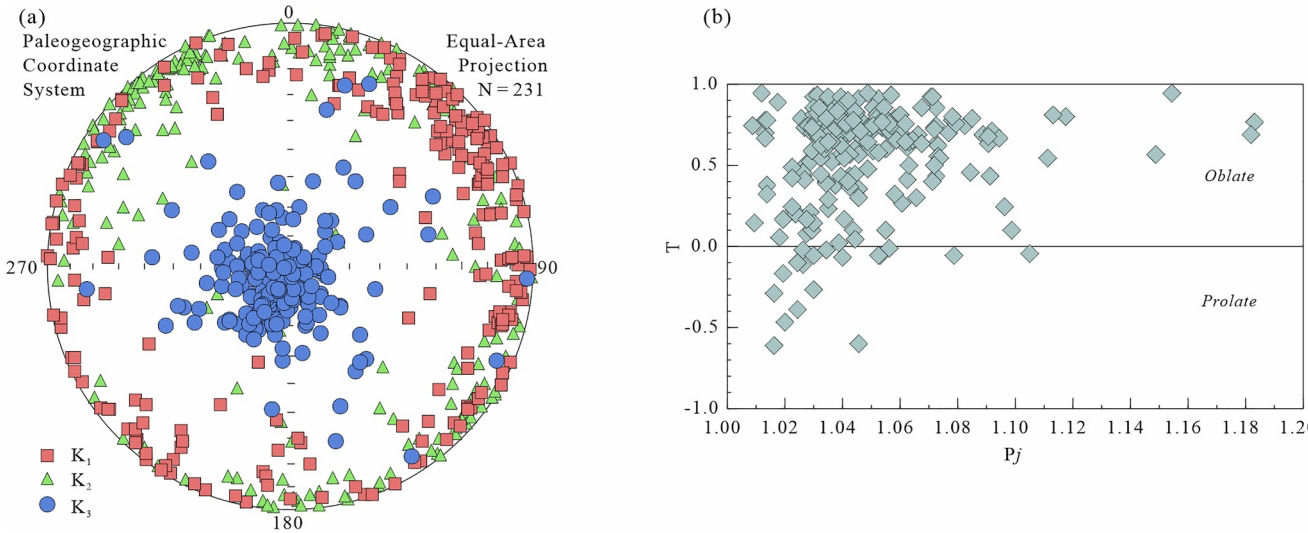

Figure 3. Anisotropy of magnetic susceptibility (AMS) of samples from Nuoyinhe Formation red beds. (a) Stereographic projections of principal susceptibility axes of K_{max}, K_{int}, and K_{min} in paleogeographic coordinate system, (b) Corrected AMS degree (Pj) versus AMS shape parameter (T).

All samples were treated by thermal demagnetization using a TD-48 thermal demagnetization furnace. The remanent magnetization was measured by 2G-755 R low-temperature superconducting magnetometer. Demagnetization steps ranged from 50 to 100°C below 500°C, and 5–30°C until 690°C. Demagnetization and remanence measurements were performed in a magnetically shielded space in which the residual field was less than 300 nT. Paleomagnetic data analysis was conducted using the online portal Paleomagnetism.org (Koymans et al., 2016, 2020). The demagnetization results were performed on the orthogonal vector diagram (Zijderveld, 1967) and principal component analysis (Kirschvink, 1980) to determine the magnetic components. Site mean paleomagnetic directions were calculated using standard Fisher statistics (Fisher, 1953) on virtual paleomagnetic poles. All paleomagnetic data were recalculated to a common reference site (37.5°N/99.1°E) for paleolatitudinal comparison and further discussion on tectonic implications.

4. Results

4.1. Detrital Zircon Morphology and Zircon U-Pb Ages

A total of 100 detrital zircon grains were analyzed and yielded 84 concordant ages with discordance of 10% or less (Table S1). The age of the zircons varies from 2,706 to 256 Ma, and a single zircon grain gives the youngest age as 256 ± 6 Ma (Figure S2 in Supporting Information S1; Table S1), which falls within the biostratigraphically determined late Permian (Lopingian) age of the Nuoyinhe Group.

4.2. Anisotropy of Magnetic Susceptibility

In tilt-corrected coordinates, the AMS data show nearly horizontal K_1 axes (D = 44.8°, I = 8.8°) and K_2 axes (D = 314.7°, I = 0.8°) and nearly vertical K_3 axes (D = 218.6°, I = 82.6°) (Figure 3a). The results indicated a bedding-parallel magnetic fabric that is consistent with compaction following sedimentation. The anisotropy degree (Pj) ranges from 1.009 to 1.183 with an average value of 1.048, and most samples have distribution between the anisotropy shape factor (T) from 0 to 1, except for 18 specimens ranging from −1 to 0 (Figure 3b). This suggests that at least at the sampling scale, the rocks have not experienced intense deformation since their formation. In general, the characteristics of ellipsoids are well-explained by deposition and compaction, indicating that the primary sedimentary fabrics are not overprinted by tectonic deformation, but that inclination shallowing because of compaction is expected.

4.3. Rock Magnetic Results

Rock magnetic experiments were designed to identify the magnetic minerals within the rocks. The IRM curves increase gradually with the increase of the magnetic field and do not reach saturation at 2.5 T (Figures 4a–4c). The

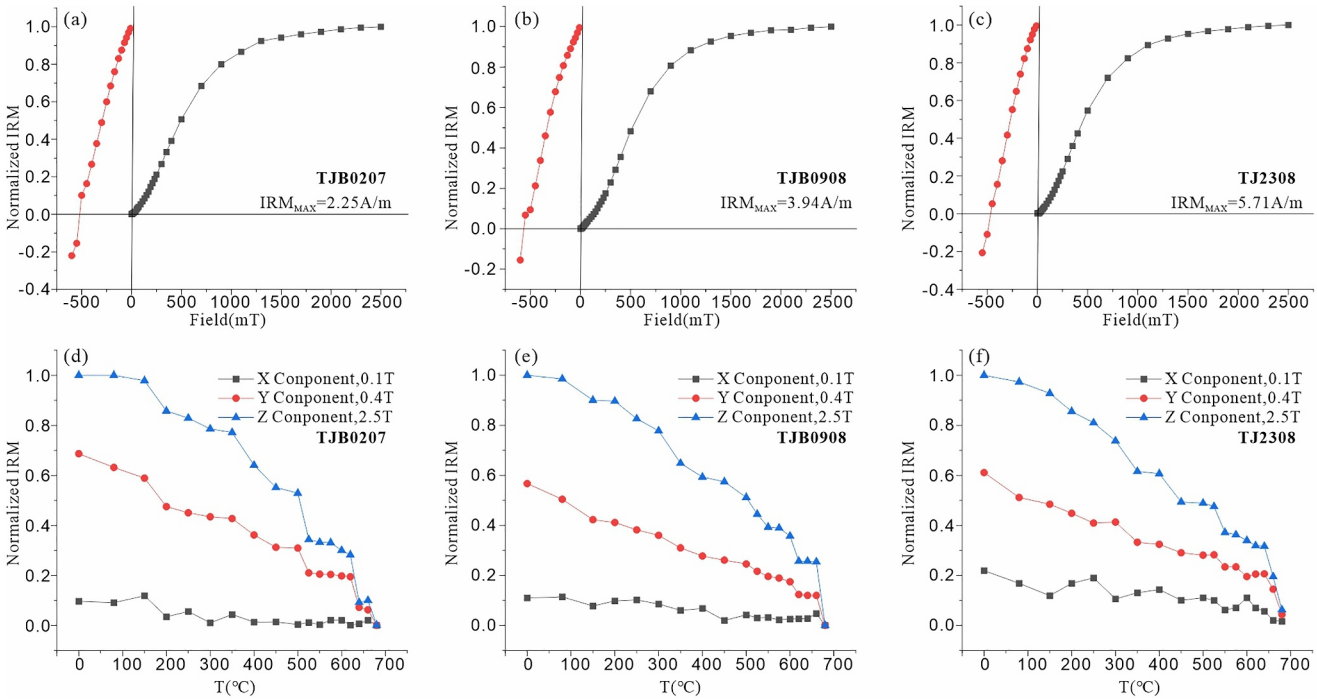

Figure 4. Rock magnetic analyses of samples from the Nuoyinhe Group. (a–c) Isothermal remanent magnetization (IRM) acquisition curves and backfield demagnetization of saturation IRM curves of representative samples; (d–f) Thermal demagnetization of three-axis IRM curves of representative samples.

curves of the backfield demagnetization of saturation IRM (SIRM) show a maximum remanence coercive force of ~450–550 mT (Figures 4a–4c), indicative of the dominance of high-coercivity magnetic minerals in the samples. The thermal demagnetization of the composite IRM curves show that high- and medium-coercivity components are dominant, and both unblocked at ~680°C (Figures 4d–4f), which is the Néel point of high-coercivity hematite (Lowrie, 1990).

We applied SEM observation, and EDS analyses to estimate the diagenetic condition of the magnetic carriers (Figure 5). The magnetic grains in the sample of Nuoyinhe Group are subhedral to euhedral and are irregular in shape, and their boundaries are very clear (Figures 5a–5f). The EDS results indicate that the magnetic minerals in the samples are mainly iron oxides containing small amounts of titanium or not, with the absence of sulfides (Figures 5g–5l). This suggests that the magnetic minerals were not influenced by chemical alteration.

4.4. Paleomagnetic Results and Statistical Analysis

A total of 199 (out of 210) specimens that underwent stepwise thermal demagnetization yielded interpretable magnetic signals, with two remanence components (Figure 6). A lower temperature component is generally isolated between NRM and 530–560°C and yield a mean direction of Dg = 1.9 ± 2.6°, Ig = 57.4 ± 1.9°, $N = 190$, $K = 26.5$, $A^{95} = 2.0°$ in geographic coordinates that is indistinguishable from the recent field direction at the sampling location (Figure 7a) and is interpreted as a viscous remanent magnetization.

A stable higher temperature component is isolated between ~560–580 and ~620–680°C which is consistent with a hematite and titanohematite component. Demagnetization curves display a convex shape and drop to zero rapidly near the unblocking temperature of hematite (~600–680°C) (Figure 6) typical for detrital remanent magnetization demagnetization curves (Jiang et al., 2015, 2022). In some cases, demagnetization did not converge to the origin in the last several steps, which we attribute to measurement errors due to weaker NRM intensities. In such cases, the ChRM interpretation was forced to the origin.

Of the 25 sampling sites, 24 yielded interpretable results. Only one location (23TJ25) yielded unsystematic and erratic demagnetization behavior that did not reveal components converging with the origin. The location averages of the remaining 24 sampling locations are provided in Table S2. We perform the Tauxe and

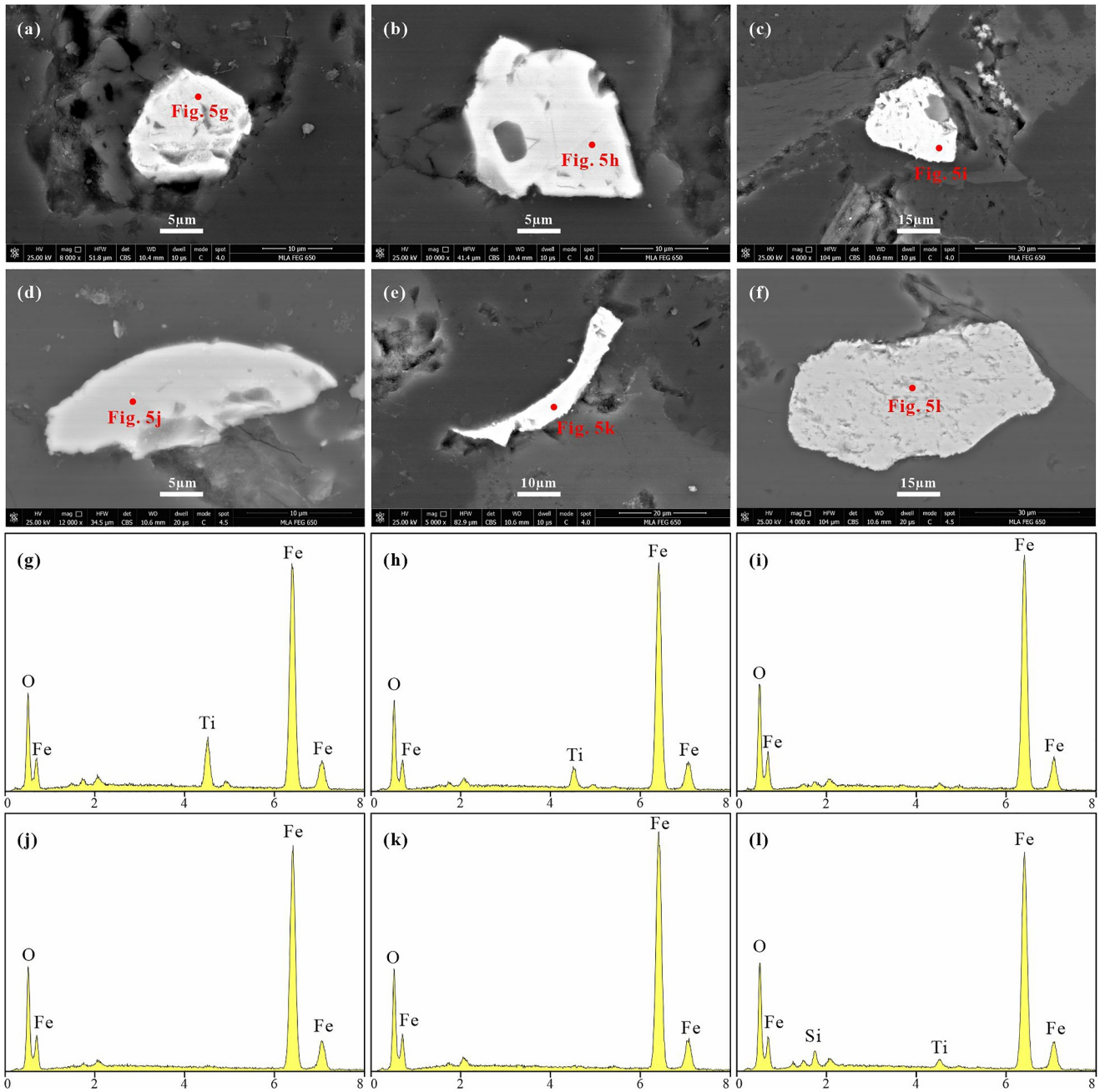

Figure 5. The morphology and elemental composition of magnetic minerals. (a–f) Scanning electron microscopy back scattered electron images. (g–l) Energy dispersive spectroscopy analyses results.

Watson (1994) fold test, which yields the highest $\tau 1$ value between 94% and 130%, and is thus positive fold, that is, optimal clustering of the data occurs after tilt correction, suggesting that the magnetization predates the folding (Figure S3 in Supporting Information S1). The fold test is also positive when applied to location averages.

To correct for inclination shallowing, the *E*/*I* correction of Tauxe and Kent (2004) compares the paleomagnetic direction scatter from a sediment-derived data set with a field model calibrated against paleomagnetic data from recent volcanic data that are free from inclination shallowing. The elongation of paleomagnetic data sets is latitude-dependent, and with each inclination comes a predicted elongation, which becomes disturbed by fattening. If the paleomagnetic data set from sedimentary rocks represents a collection of spot readings that is representative for PSV of the paleomagnetic field, the data set can be step-by-step uncompacted until inclination

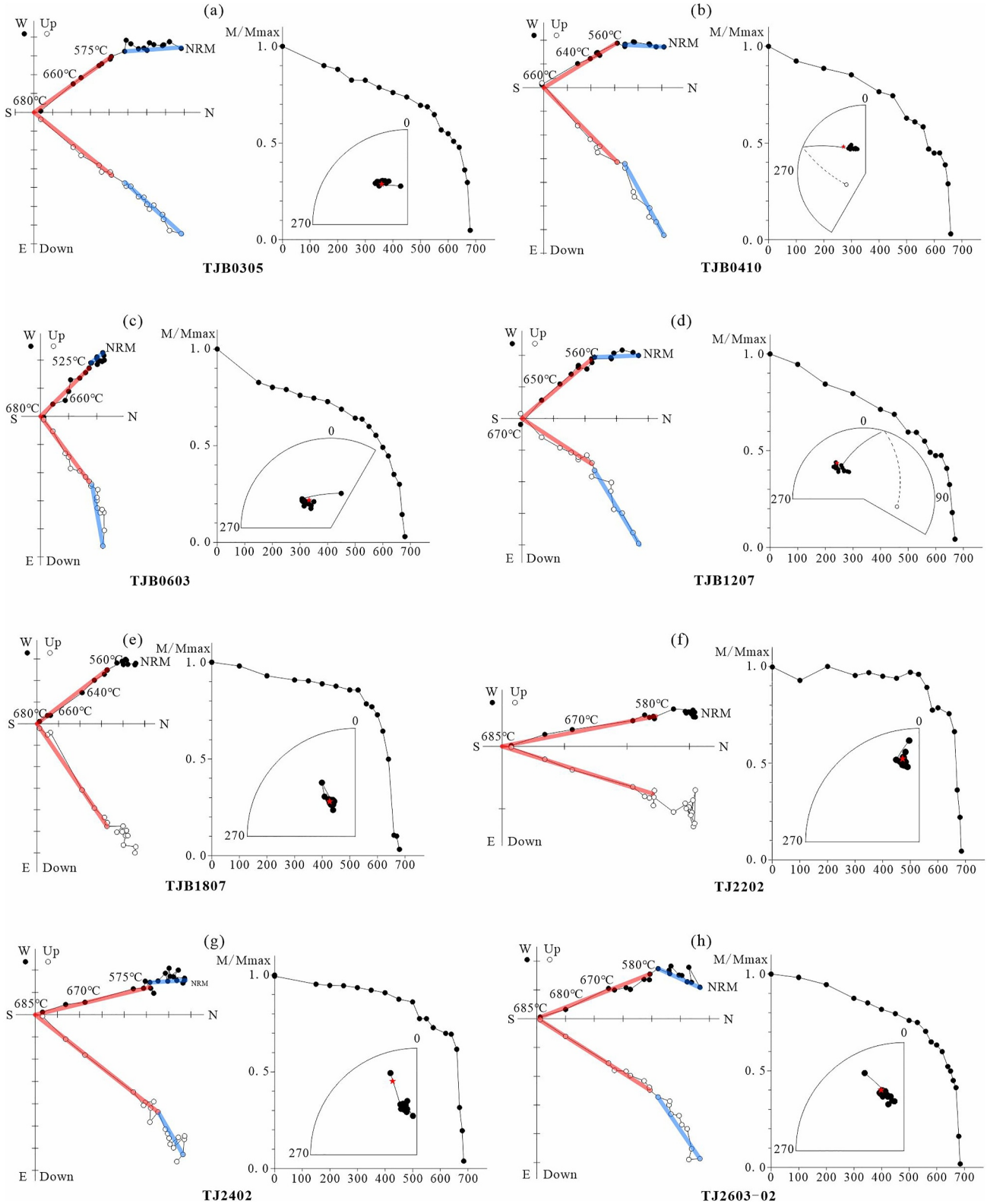

Figure 6. Representative demagnetization characteristics of samples from Nuoyinhe Group in geographic coordinates. Filled circles represent the horizontal projections, open circles represent the vertical projections. NRM is the natural remanent magnetization.

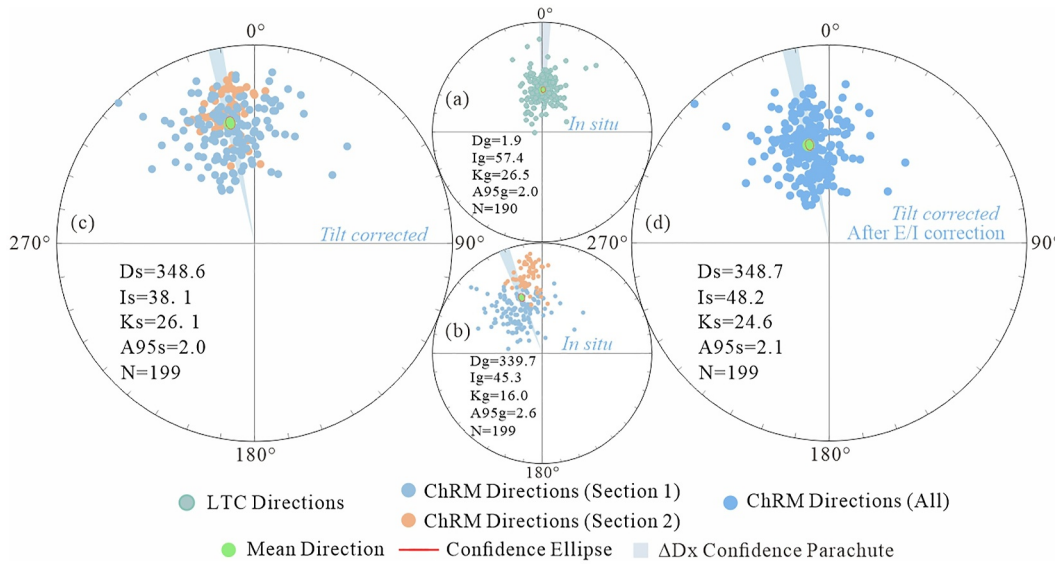

Figure 7. Paleomagnetic results from Nuoyinhe Formation. (a) Equal-area plots of the low temperature components before tilt correction. (b) Equal-area plots of the high temperature components before tilt correction. (c) Equal-area plots of the high temperature components after tilt correction. (d) Equal-area plots of the tilt corrected high temperature components after *E*/*I* correction.

and elongation are consistent with the predicted field model (Tauxe & Kent, 2004). A key unknown, however, is whether a paleomagnetic direction from a sediment core represents a spot reading of the paleomagnetic field, or whether each core already average (part of) the field, or whether multiple cores from one sedimentary horizon together represent a spot reading. Vaes et al. (2021) recently tested quantitative criteria to evaluate whether a sediment-derived data set may approximate a (compacted) PSV-induced scatter. They found that when data sets (a) exceed $N = 80$; (b) pass the Deenen et al. (2011) criteria that text whether a scatter may be straightforwardly explained by PSV, and (c) rotations within the data set do not exceed ∼15°, a sediment-derived paleomagnetic data set may be regarded as a collection of unique spot readings of the field, and be used to compute an *E*/*I* corrected paleomagnetic pole.

The total of 199 specimens yielded an overall mean direction of Dg = 339.7 ± 2.9°, Ig = 45.3 ± 3.2°, $K = 16.0$, $A_{95} = 2.6°$, in geographic coordinates and Ds = 348.6° ± 2.1°, Is = 38.1° ± 2.8°, $K = 26.1$, $A_{95} = 2.0°$ in tectonic coordinates (Figures 7b and 7c; Table S3). The declinations of the two subsections are identical and there is no reason to infer significant vertical axis rotation differences between the sampled collections. The A_{95} value falls within the n-dependent reliability envelope of Deenen et al. (2011): for $N = 199$, $A_{95\text{min, max}} = 1.4, 2.9$, so that the A_{95} of the data set may in principle be straightforwardly explained by PSV alone. And with $N > 80$, our data set fulfills the Vaes et al. (2021) criteria for successful correction of inclination shallowing using the *E*/*I* method of Tauxe and Kent (2004). This correction applied yields a flattening factor of 0.68 (Figure S4 in Supporting Information S1) and increases the inclination from 38.1 ± 2.8° to 47.0 ± 2.5°, and the corresponding paleolatitude from ∼21.4° [20.2°, 22.8°] to 28.2° [26.9°, 30.6°].

Finally, even though the total scatter passes the Deenen et al. (2011) criteria, inspection of the locality averages reveals that there is wide variation in the degree of scatter. Some localities have K-values well over 100, suggesting that there, the collection of directions may reproduce the same spot reding of the paleomagnetic field. To evaluate whether a possible bias of such low-scatter localities would significantly influence the paleolatitude predicted by the E/I correction, we performed a test in which directions for locations with $k > 100$ was represented by a single direction in the total data set. This lowered N to 133 and generated a somewhat higher flattening factor of 0.63, and predicted a paleolatitude of 33.7° [21.9°, 35.6°], that is, a few degrees higher than when using all data as individual readings. This small difference has no impact on the discussion and conclusions below.

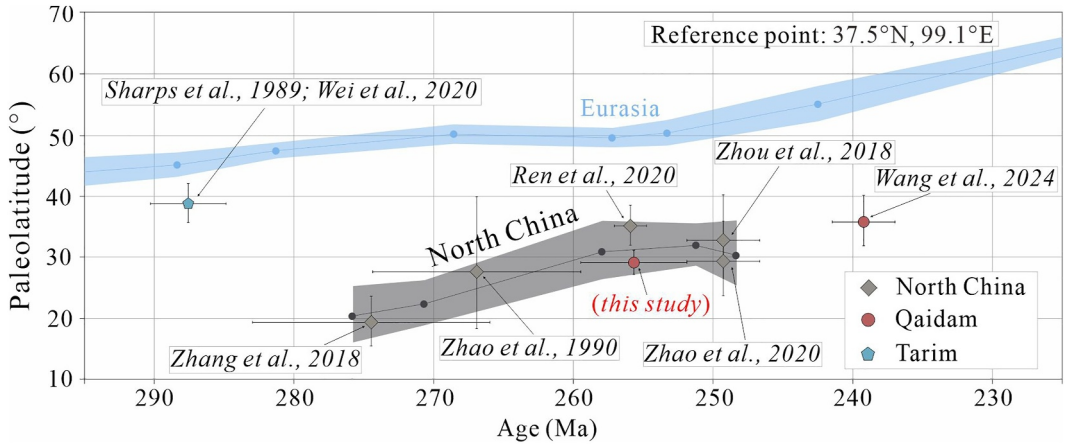

Figure 8. Paleolatitudinal comparison with Eurasia, North China, Tarim, and Qaidam during the Permo-Triassic. The paleolatitude evolution was calculated and drawn using the online tools APWP-Online.org (Vaes et al., 2024) and paleomagnetism.org (Koymans et al., 2016, 2020), respectively.

5. Discussion

5.1. Paleolatitudinal Position of the Qaidam Block

We compute a difference between our new paleomagnetic pole for the Upper Permian of the Qaidam Block and the global APWP of Eurasia (Vaes et al., 2023) using the online tool APWP-Online.org (Vaes et al., 2024). This tool weighs the uncertainty of the global APWP against the number of directions used for the reference pole, which generates a 95% certainty that a significant difference is geologically meaningful (Vaes et al., 2022). Our Late Permian Qaidam pole differs significantly from Eurasia paleomagnetic data in both declination (suggesting a counterclockwise vertical axis rotation component of $60 \pm 4°$) and inclination (Figures S5a and S5b in Supporting Information S1). The latter demonstrates that the Qaidam Block was located at a paleolatitudinal distance of $21° \pm 2°$ (i.e., ~2,300 ± 220 km) south of Eurasia in the late Permian (255.7 ± 3.8 Ma) (Figure S5b in Supporting Information S1). A recently published Triassic pole of B. Wang et al. (2024) for the early Triassic (239.3 ± 2.3 Ma) reveals a similar paleolatitudinal separation of 19 ± 8° (Figure S5b in Supporting Information S1).

Conversely, the Qaidam poles plot close to the paleomagnetic directions expected for the North China Block (Figure S5c in Supporting Information S1). The apparent polar wander path for North China in the Permian is determined by five paleomagnetic poles, three from volcanic rocks and two from inclination-shallowing-corrected sedimentary rocks, with ages range ~275–250 Ma (Figure 8; Table S4). Our new Qaidam pole for the late Permian, as well as the Triassic pole of B. Wang et al. (2024) are indistinguishable from the North China paleolatitudes computed for on our reference location from the published poles using the approach of Vaes et al. (2022, 2024) ($2.2° \pm 3.5°$ and $3.2° \pm 5.3°$, respectively) (Figure S5c in Supporting Information S1). In other words, the paleolatitudes from the Qaidam Block are straightforwardly explained if they traveled on the same tectonic plate as the North China Block since the late Permian, until the two converged ~150 km during the Cenozoic shortening of NE Tibet (van Hinsbergen et al., 2011). Our Late Permian pole also reveals a clockwise rotation of ~20° relative to North China, and the Triassic pole of B. Wang et al. (2024) suggests a clockwise rotation of as much as 90° relative to North China (Figure S5d in Supporting Information S1). These rotations, however, may well result from the intense Cenozoic deformation of the margins of the Qaidam Block where these poles were collected, and do not necessitate inferring major post-Permian plate motion differences between Qaidam and North China. Finally, a minor relative motion between the Qaidam Block and North China is consistent with the interpretation that the late Permian to Triassic Kunlun arc that fringes Qaidam to the south is contiguous with the contemporaneous arc on the southern North China Block along the Qinling-Dabie suture zone (Dong et al., 2011).

The Tarim Basin has undergone some Cenozoic motion relative to Eurasia since its Permian accretion. This motion culminated in a 10° vertical axis rotation around a pole in the NE of the basin, leading to westward increasing Miocene shortening in the Tien Shan (van Hinsbergen et al., 2011; Yin et al., 1998). However, this

motion did not change the paleolatitudinal position of the Tarim Basin relative to Eurasia by more than 1–2° and the modern position relative to Eurasia should thus closely resemble the position following Permian accretion. Additionally, the Qaidam Block had a northward motion component of ∼150 km, or ∼1.5°, during ∼400 km of Cenozoic strike-slip motion along the Altyn Tagh Fault (Cowgill et al., 2003; van Hinsbergen et al., 2011). Hence, these Cenozoic motions explain only a fraction of post-Permian convergence between Qaidam and Eurasia.

An Early Permian paleomagnetic pole from the Tarim Basin (Sharps et al., 1989; Wei et al., 2020) that shortly predates the Permian suturing in of the Tien Shan reveals a paleolatitudinal difference with Eurasia of only 6.6° ± 3.8°, showing proximity of the Tarim Block to Eurasia by that time (Figure 8), where geological data suggest final collision by late Permian time (Xiao et al., 2013, 2020). As a result, the paleolatitudinal separation of ∼20° that follows from our data set strongly suggests that major convergence occurred between the Qaidam Block and the Tarim Block since the late Permian. Paleomagnetic data from the Tarim Block from Permian and younger time have often shown paleolatitudes that are lower than those predicted for Eurasia at respective sampling locations (e.g., Gilder et al., 2008). If these accurately reflect paleolatitude, part of the 20° post-Permian convergence between Qaidam and Eurasia must have been accommodated in the Tien Shan region. However, those poles come from sedimentary rocks that were not corrected for compaction-induced inclination shallowing, and these paleolatitudes are thus too low. Because the original data remain unpublished, no quantitative evaluation is possible. Given this, we consider it likely that the plate boundary between the North China/Qaidam and Eurasian continents after the Permian is best sought within the Tarim Basin, or between the Tarim and Qaidam Blocks.

5.2. Paleogeographic Evolution of Mesozoic Assembly of Eurasia

Previous paleogeographic reconstructions have realized that the reconstruction of the Mongol-Okhotsk Ocean, as well as the Solonker Ocean that closed earlier, in the Triassic, within the Central Asian Orogenic Belt (Eizenhöfer & Zhao, 2018; Xiao et al., 2003), required relative plate motion between the North China and Tarim Blocks (Figure 9; Huang et al., 2018; Van der Voo et al., 2015). The paleomagnetic data reveal that motion must have involved a northward motion of North China and Qaidam relative to Eurasia of at least ∼20°, that is, >2,000 km, between the late Permian and the latest Jurassic (Figure 8). It is possible that this motion involved an important component of transform motion between the Qaidam and Tarim Blocks, but previous paleogeographic models systematically also show significant convergence that inevitably requires subduction. To the northeast, this cryptic plate boundary must first have connected the western Solonker subduction zone that was identified between the North China Block and the Central Asian accretionary orogenic belt until the late Triassic (Eizenhöfer & Zhao, 2018; Xiao et al., 2003, 2015). Later, this plate boundary must somehow have connected to the Mongol-Okhotsk subduction zones. This latter plate boundary may have involved the well-documented East Gobi Fault Zone that accommodated 200 km of the late Triassic transform motion (Figure 1a; Heumann et al., 2014) but may have been diffuse as the East Asian Orogenic Belt rotated and closed the Mongol-Okhotsk Ocean as an orocline (Van der Voo et al., 2015; T. Wang et al., 2022).

To the southwest, the cryptic plate boundary between the Qaidam and Tarim Blocks must have continued toward the Pamirs and Afghanistan to merge with the Paleotethys subduction zone until the late Triassic, and with younger Tethyan subduction zones to the south thereafter (Kapp & DeCelles, 2019). One possible candidate where this suture could connect to is the latest Jurassic-earliest Cretaceous Waser Suture zone that separates the Cimmerian Helmand Block of Afghanistan from Eurasia (Şengör et al., 1991; Siehl, 2017; Tapponnier et al., 1981). In addition, the Silk Road Arc magmatic arc system that extended at least into the Triassic was postulated on the southern Eurasian margin that connected through the southern Tarim Block toward the northeast, along the plate boundary for which we identify the need in our paper (Natal'in and Şengör, 2005). These are interesting leads to pursue the fate of the final intra-Asian plate boundary further, but this awaits a detailed reconstruction of the Afghan and Iranian orogen, as well as the (Inner) Mongolian continuations and terminations of known suture zones, and their integration in the kinematic evolution of Tibet and the Pamirs.

Our analysis illustrates how a full understanding of Eurasian assembly requires the detailed study of the paleo-plate boundaries that must have connected the Mongol-Okhotsk and the Tethyan subduction zones. However, what we consider the most puzzling implication of our results is that a former, long-lived, major plate boundary that likely involved a component of subduction must somehow be hidden around the region of the modern Alty Tagh Fault or the Tarim Basin. The consistency between our finding and available paleomagnetic data for the North China Block for the Permian, and the long-standing evidence that North China-Eurasia motion continued

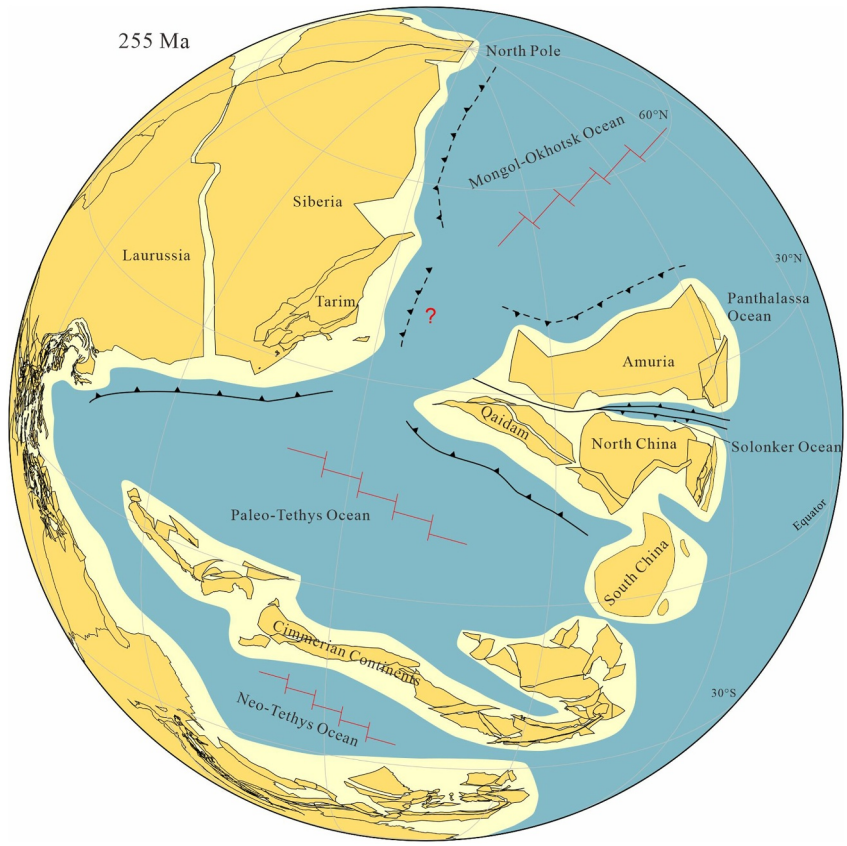

Figure 9. Schematic paleogeographic reconstruction of the East Asian blocks, Laurussia and Siberia. The Qaidam Block is positioned according to the data in this study. Amuria, South China, Cimmeria, the Tethyan oceans, and the major continents follow reconstructions of Ren et al. (2020), Huang et al. (2018), Torsvik and Cocks (2017), Advokaat and van Hinsbergen. (2024), P. P. Song et al. (2017), and van Hinsbergen et al. (2020), placed in the paleomagnetic reference frame of Vaes et al. (2023).

until the latest Jurassic (Cogné et al., 2005; Van der Voo et al., 2015) leaves little room for alternative interpretations. For now, we may only speculate whether and why there is no rock record recognized at the suture of this long-lasting plate boundary. Perhaps it lies buried below the Tarim Basin or lies over thrusted below the Tibetan Plateau. Nonetheless, resolving these issues is key for reconstruction of assembly of continents in general, and Eurasia specifically.

6. Conclusions

Paleomagnetic data have long shown that the North China Block converged with Eurasia prior to its latest Jurassic accretion during the closure of the Mongol-Okhotsk Ocean, but when and how this motion was accommodated to the west, between North China and Tarim, remains poorly known. Here, we show new paleomagnetic data from Permian sandstones from the Qaidam Block of northern Tibet, adjacent to the Tarim Basin and separated from North China by a Cenozoic fold-thrust belt. Our results reveal a hematite-carried magnetization that we interpret as primary based on a rock magnetic analysis, statistical behavior that fits recording paleosecular variation, and a positive fold test. We corrected our data for inclination shallowing with the *E*/*I* method and arrive at a paleomagnetic pole of $D = 348.7° \pm 2.3°$, $I = 47° \pm 2.5°$, $\lambda = 77.6°$N, $\phi = 332.8°$E, $A_{95} = 2.1°$, $K = 24.7$, $N = 199$. These data reveal that the paleolatitude is ~20° lower than predicted by the Eurasian apparent polar wander path for the reference location. We conclude that a cryptic plate boundary that somehow connected the Mongol-Okhotsk subduction zones with the Tethyan subduction zones must have existed between the Qaidam and Tarim Blocks in Mesozoic time. The detailed reconstruction of this boundary is a key contribution to the final amalgamation of the Eurasian continental land mass.

Data Availability Statement

The supporting data of this study are available in Supporting Information S1, which are also can be found in Zhou (2025).

Acknowledgments
We thank Mark Dekkers for discussing the rock magnetic and paleomagnetic results. We are also deeply grateful to Editor Alexandre Schubnel, Associate Editor Daniel Pastor-Galán, and the three anonymous reviewers for their constructive comments and suggestions, which have significantly improved this manuscript. This study was supported by the National Natural Science Foundation of China (Grants 42372251, 42074075, 91855211, 42274097, 423722253) and the China Scholarship Council (202306970045).

References

Advokaat, E. L., & van Hinsbergen, D. J. J. (2024). Finding Argoland: Reconstructing a microcontinental archipelago from the SE Asian accretionary orogen. *Gondwana Research*, *128*, 161–263. https://doi.org/10.1016/j.gr.2023.10.005

Allen, M., Windley, B., & Zhang, C. (1993). Palaeozoic collisional tectonics and magmatism of the Chinese Tien Shan, central Asia. *Tectonophysics*, *220*(1–4), 89–115. https://doi.org/10.1016/0040-1951(93)90225-9

Cawood, P. A., Kröner, A., Collins, W. J., Kusky, T. M., Mooney, W. D., & Windley, B. F. (2009). Accretionary orogens through Earth history. *Geological Society, London, Special Publications*, *318*(1), 1–36. https://doi.org/10.1144/SP318.1

Cogné, J. P., Kravchinsky, V. A., Halim, N., & Hankard, F. (2005). Late Jurassic-Early Cretaceous closure of the Mongol-Okhotsk Ocean demonstrated by new Mesozoic palaeomagnetic results from the Trans-Baikal area (SE Siberia). *Geophysical Journal International*, *163*(2), 813–832. https://doi.org/10.1111/j.1365-246X.2005.02782.x

Cowgill, E., Yin, A., Harrison, T. M., & Wang, X. F. (2003). Reconstruction of the Altyn Tagh fault based on U-Pb geochronology: Role of back thrusts, mantle sutures, and heterogenoous crustal strength in forming the Tibetan Plateau. *Journal of Geophysical Research: Solid Earth*, *108*, 2346. https://doi.org/10.1029/2002JB002080

Deenen, M. H., Langereis, C. G., van Hinsbergen, D. J., & Biggin, A. J. (2011). Geomagnetic secular variation and the statistics of palaeomagnetic directions. *Geophysical Journal International*, *186*(2), 509–520. https://doi.org/10.1111/j.1365-246X.2011.05050.x

Dong, Y. P., He, D., Sun, S., Liu, X., Zhou, X., Zhang, F., et al. (2018). Subduction and accretionary tectonics of the East Kunlun orogen, western segment of the Central China Orogenic System. *Earth-Science Reviews*, *186*, 231–261. https://doi.org/10.1016/j.earscirev.2017.12.006

Dong, Y. P., Zhang, G. W., Neubauer, F., Liu, X. M., Genser, J., & Hauzenberger, C. (2011). Tectonic evolution of the Qinling orogen, China: Review and synthesis. *Journal of Asian Earth Sciences*, *41*(3), 213–237. https://doi.org/10.1016/j.jseaes.2011.03.002

Eizenhöfer, P. R., & Zhao, G. (2018). Solonker Suture in East Asia and its bearing on the final closure of the eastern segment of the Palaeo-Asian Ocean. *Earth-Science Reviews*, *186*, 153–172. https://doi.org/10.1016/j.earscirev.2017.09.010

Eizenhöfer, P. R., Zhao, G., Zhang, J., & Sun, M. (2014). Final closure of the Paleo-Asian Ocean along the Solonker suture zone: Constraints from geochronological and geochemical data of Permian volcanic and sedimentary rocks. *Tectonics*, *33*(4), 441–463. https://doi.org/10.1002/2013TC003357

Fisher, R. A. (1953). Dispersion on a sphere, Proceedings of the Royal Society of London. Series A. *Mathematical and Physical Sciences*, *217*(1130), 295–305. https://doi.org/10.1098/rspa.1953.0064

Gilder, S. A., Gomezx, J., Chen, Y., & Cogné, J. P. (2008). A new paleogeographic configuration of the Eurasian landmass resolves a paleomagnetic paradox of the Tarim Basin (China). *Tectonics*, *27*(1), TC1012. https://doi.org/10.1029/2007TC002155

Heumann, M. J., Johnson, C. L., Webb, L. E., Taylor, J. P., Jalbaa, U., & Minjin, C. (2014). Total and incremental left-lateral displacement across the East Gobi Fault Zone, southern Mongolia: Implications for timing and modes of polyphase intracontinental deformation. *Earth and Planetary Science Letters*, *392*, 1–15. https://doi.org/10.1016/j.epsl.2014.01.016

Huang, B., Yan, Y., Piper, J. D., Zhang, D., Yi, Z., Yu, S., & Zhou, T. (2018). Paleomagnetic constraints on the paleogeography of the East Asian blocks during late Paleozoic and early Mesozoic times. *Earth-Science Reviews*, *186*, 8–36. https://doi.org/10.1016/j.earscirev.2018.02.004

Isozaki, Y., Maruyama, S., & Furuoka, F. (1990). Accreted oceanic materials in Japan. *Tectonophysics*, *181*(1–4), 179–205. https://doi.org/10.1016/0040-1951(90)90016-2

Jiang, Z., Liu, Q., Dekkers, M. J., Tauxe, L., Qin, H., Barrón, V., & Torrent, J. (2015). Acquisition of chemical remanent magnetization during experimental ferrihydrite–hematite conversion in Earth-like magnetic field—implications for paleomagnetic studies of red beds. *Earth and Planetary Science Letters*, *428*, 1–10. https://doi.org/10.1016/j.epsl.2015.07.024

Jiang, Z., Liu, Q., Roberts, A. P., Dekkers, M. J., Barrón, V., Torrent, J., & Li, S. (2022). The magnetic and color reflectance properties of hematite: From Earth to Mars. *Reviews of Geophysics*, *60*(1), e2020RG000698. https://doi.org/10.1029/2020RG000698

Jolivet, M., Arzhannikova, A., Frolov, A., Arzhannikov, S., Kulagina, N., Akulova, V., & Vassallo, R. (2017). Late Jurassic-Early Cretaceous paleoenvironmental evolution of the Transbaikal basins (SE Siberia): Implications for the Mongol-Okhotsk orogeny. *Bulletin de la Societe Geologique de France*, *188*(1–2), 1–22. https://doi.org/10.1051/bsgf/2017010

Kapp, P., & DeCelles, P. G. (2019). Mesozoic–Cenozoic geological evolution of the Himalayan-Tibetan orogen and working tectonic hypotheses. *American Journal of Science*, *319*(3), 159–254. https://doi.org/10.2475/03.2019.01

Kirschvink, J. (1980). The least-squares line and plane and the analysis of palaeomagnetic data. *Geophysical Journal International*, *62*(3), 699–718. https://doi.org/10.1111/j.1365-246X.1980.tb02601.x

Koymans, M. R., Langereis, C. G., Pastor-Galán, D., & van Hinsbergen, D. J. (2016). Paleomagnetism.org: An online multi-platform open-source environment for paleomagnetic data analysis. *Computers & Geoscience*, *93*, 127–137. https://doi.org/10.1016/j.cageo.2016.05.007

Koymans, M. R., van Hinsbergen, D. J., Pastor-Galán, D., Vaes, B., & Langereis, C. (2020). Towards FAIR paleomagnetic data management through Paleomagnetism.org 2.0. *Geochemistry, Geophysics, Geosystems*, *21*(2), e2019GC008838. https://doi.org/10.1029/2019GC008838

Liu, G. (1980). Permian strata and paleontological characteristics in Buha River valley, Tianjun district, Qinghai. *Qinghai Geology*, *1*, 1–22. (in Chinese with English abstract).

Lowrie, W. (1990). Identification of ferromagnetic minerals in a rock by coercivity and unblocking temperature properties. *Geophysical Research Letters*, *17*(2), 159–162. https://doi.org/10.1029/GL017i002p00159

Lu, Y. (1986). Permian lamellibranchs from Buha River valley, Tianjun district, Qinghai. *Acta Palaeontologica Sinica*, *25*(4), 463–473. (in Chinese with English abstract).

Ludwig, K. R. (2003). User's manual for IsoPlot 3.0, A geochronological toolkit for Microsoft Excel, 71.

Natal'in, B. A., & Şengör, A. C. (2005). Late Palaeozoic to Triassic evolution of the Turan and Scythian platforms: The pre-history of the Palaeo-Tethyan closure. *Tectonophysics*, *404*(3–4), 175–202. https://doi.org/10.1016/j.tecto.2005.04.011

QBGMR (Qinghai Bureau of Geology and Mineral Resources). (1976). Regional geological investigation of the Xiahuancang Area, Beijing: Regional geology of Qinghai Province supply paper (pp. 1–102). (in Chinese).

Ren, Q., Zhang, S., Gao, Y., Zhao, H., Wu, H., Yang, T., & Li, H. (2020). New Middle–Late Permian paleomagnetic and geochronological results from Inner Mongolia and their paleogeographic implications. *Journal of Geophysical Research: Solid Earth*, *125*(7), e2019JB019114. https://doi.org/10.1029/2019JB019114

Şengör, A., Cin, A., Rowley, D. B., & Nie, S. Y. (1991). Magmatic evolution of the tethysides: A guide to reconstruction of collage history. *Palaeogeography, Palaeoclimatology, Palaeoecology*, *89*(1–4), 411–440. https://doi.org/10.1016/0031-0182(91)90143-F

Şengör, A., Natal'In, B., & Burtman, V. (1993). Evolution of the Altaid tectonic collage and Palaeozoic crustal growth in Eurasia. *Nature*, *364*(6435), 299–307. https://doi.org/10.1038/364299a0

Sharps, R., McWilliams, M., Li, Y., Cox, A., Zhang, Z., Zhai, Y., et al. (1989). Lower Permian paleomagnetism of the Tarim block, northwestern China. *Earth and Planetary Science Letters*, *92*(3–4), 275–291. https://doi.org/10.1016/0012-821X(89)90052-6

Siehl, A. (2017). Structural setting and evolution of the Afghan orogenic segment—A review. *Geological Society, London, Special Publications*, *427*(1), 57–88. https://doi.org/10.1144/SP427.8

Sobel, E. R., & Arnaud, N. (1999). A possible middle Paleozoic suture in the Altyn Tagh, NW China. *Tectonics*, *18*(1), 64–74. https://doi.org/10.1029/1998TC900023

Song, D., Xiao, W., Collins, A. S., Glorie, S., Han, C., & Li, Y. (2018). Final subduction processes of the Paleo-Asian Ocean in the Alxa Tectonic Belt (NW China): Constraints from field and chronological data of Permian arc-related volcano-sedimentary rocks. *Tectonics*, *37*(6), 1658–1687. https://doi.org/10.1029/2017TC004919

Song, P. P., Ding, L., Li, Z. Y., Lippert, P. C., & Yue, Y. H. (2017). An early bird from Gondwana: Paleomagnetism of Lower Permian lavas from northern Qiangtang (Tibet) and the geography of the Paleo-Tethys. *Earth and Planetary Science Letters*, *475*, 119–133. https://doi.org/10.1016/j.epsl.2017.07.023

Tapponnier, P., Mattauer, M., Proust, F., & Cassaigneau, C. (1981). Mesozoic ophiolites, sutures, and arge-scale tectonic movements in Afghanistan. *Earth and Planetary Science Letters*, *52*(2), 355–371. https://doi.org/10.1016/0012-821X(81)90189-8

Tauxe, L., & Kent, D. V. (2004). A simplified statistical model for the geomagnetic field and the detection of shallow bias in paleomagnetic inclinations: Was the ancient magnetic field dipolar? *Geophysical monograph*, *145*, 101–115. https://doi.org/10.1029/145GM08

Tauxe, L., & Watson, G. (1994). The fold test: An eigen analysis approach. *Earth and Planetary Science Letters*, *122*(3–4), 331–341. https://doi.org/10.1016/0012-821X(94)90006-X

Torsvik, T. H., & Cocks, L. R. M. (2017). *Earth history and palaeogeography* (p. 317). Cambridge University Press.

Vaes, B., Gallo, L. C., & van Hinsbergen, D. J. (2022). On pole position: Causes of dispersion of the paleomagnetic poles behind apparent polar wander paths. *Journal of Geophysical Research: Solid Earth*, *127*(4), e2022JB023953. https://doi.org/10.1029/2022JB023953

Vaes, B., Li, S., Langereis, C. G., & van Hinsbergen, D. J. (2021). Reliability of palaeomagnetic poles from sedimentary rocks. *Geophysical Journal International*, *225*(2), 1281–1303. https://doi.org/10.1093/gji/ggab016

Vaes, B., van Hinsbergen, D. J., & Paridaens, J. (2024). APWP-online.org: A global reference database and open-source tools for calculating apparent polar wander paths and relative paleomagnetic displacements. *Tektonika*, *2*(1), 174–189. https://doi.org/10.55575/tektonika2024.2.1.44

Vaes, B., van Hinsbergen, D. J., van de Lagemaat, S. H., van der Wiel, E., Lom, N., Advokaat, E. L., et al. (2023). A global apparent polar wander path for the last 320 Ma calculated from site-level paleomagnetic data. *Earth-Science Reviews*, *245*, 104547. https://doi.org/10.1016/j.earscirev.2023.104547

Van der Meer, D. G., Van Hinsbergen, D. J., & Spakman, W. (2018). Atlas of the underworld: Slab remnants in the mantle, their sinking history, and a new outlook on lower mantle viscosity. *Tectonophysics*, *723*, 309–448. https://doi.org/10.1016/j.tecto.2017.10.004

Van der Voo, R., van Hinsbergen, D. J., Domeier, M., Spakman, W., & Torsvik, T. H. (2015). Latest Jurassic–earliest Cretaceous closure of the Mongol-Okhotsk Ocean: A paleomagnetic and seismological-tomographic analysis. *Geological Society of America Special Paper*, *513*, 589–606. https://doi.org/10.1130/2015.2513(19)

van Hinsbergen, D. J. J. (2022). Indian plate paleogeography, subduction and horizontal underthrusting below Tibet: Paradoxes, controversies and opportunities. *National Science Review*, *9*(8), nwac074. https://doi.org/10.1093/nsr/nwac074

van Hinsbergen, D. J. J., Kapp, P., Dupont-Nivet, G., Lippert, P. C., DeCelles, P. G., & Torsvik, T. H. (2011). Restoration of Cenozoic deformation in Asia and the size of Greater India. *Tectonics*, *30*(5), TC5003. https://doi.org/10.1029/2011TC002908

van Hinsbergen, D. J. J., Torsvik, T. H., Schmid, S. M., Matenco, L., Maffione, M., Vissers, R. L. M., et al. (2020). Orogenic architecture of the Mediterranean region and kinematic reconstruction of its tectonic evolution since the Triassic. *Gondwana Research*, *81*, 79–229. https://doi.org/10.1016/j.gr.2019.07.009

Wang, B., Huang, B., Yang, Z., Zhang, G., Liu, X., Duan, L., et al. (2024). Palaeomagnetic results from early Mesozoic strata in the Qaidam Basin and their implications for the formation of the Northern China Domain. *Geophysical Journal International*, *236*(3), 1621–1635. https://doi.org/10.1093/gji/ggad496

Wang, T., Tong, Y., Xiao, W., Guo, L., Windley, B. F., Donskaya, T., et al. (2022). Rollback, scissor-like closure of the Mongol-Okhotsk Ocean and formation of an orocline: Magmatic migration based on a large archive of age data. *National Science Review*, *9*(5), nwab210. https://doi.org/10.1093/nsr/nwab210

Wang, T., Zhou, Y., Chai, R., Cheng, X., Wang, P., Xing, L., et al. (2023). Microcontinental block amalgamation in the northern Tibetan Plateau and its significance for understanding the closure of the Proto-Tethyan Ocean. *Palaeogeography, Palaeoclimatology, Palaeoecology*, *627*, 111722. https://doi.org/10.1016/j.palaeo.2023.111722

Wei, B., Yang, X., Cheng, X., Domeier, M., Wu, H., Kravchinsky, V. A., et al. (2020). An absolute paleogeographic positioning of the early Permian Tarim large igneous province. *Journal of Geophysical Research: Solid Earth*, *125*(5), e2019JB019111. https://doi.org/10.1029/2019JB019111

Xiao, W., Song, D., Windley, B. F., Li, J., Han, C., Wan, B., et al. (2020). Accretionary processes and metallogenesis of the Central Asian Orogenic Belt: Advances and perspectives. *Science China Earth Sciences*, *63*(3), 329–361. https://doi.org/10.1007/s11430-019-9524-6

Xiao, W., Windley, B. F., Allen, M. B., & Han, C. (2013). Paleozoic multiple accretionary and collisional tectonics of the Chinese Tianshan orogenic collage. *Gondwana Research*, *23*(4), 1316–1341. https://doi.org/10.1016/j.gr.2012.01.012

Xiao, W., Windley, B. F., Hao, J., & Zhai, M. (2003). Accretion leading to collision and the Permian Solonker suture, Inner Mongolia, China: Termination of the central Asian orogenic belt. *Tectonics*, *22*(6), 1069. https://doi.org/10.1029/2002TC001484

Xiao, W., Windley, B. F., Sun, S., Li, J., Huang, B., Han, C., et al. (2015). A tale of amalgamation of three Permo-Triassic collage systems in Central Asia: Oroclines, sutures, and terminal accretion. *Annual Review of Earth and Planetary Sciences*, *43*(1), 477–507. https://doi.org/10.1146/annurev-earth-060614-105254

Xu, W., Sun, Z., Pei, J., Pan, J., Li, H., Li, A., et al. (2011). New late Permian paleomagnetic results from Qaidam block and tectonic implications. *Acta Petrologica Sinica*, *27*(11), 3479–3486. (in Chinese with English abstract).

Yin, A., & Harrison, T. M. (2000). Geologic evolution of the Himalayan-Tibetan orogen. *Annual Review of Earth and Planetary Sciences*, *28*(1), 211–280. https://doi.org/10.1146/annurev.earth.28.1.211

Yin, A., Nie, S., Craig, T. M., Harrison, T. M., Qian, X. L., Yang, G., & Geng, Y. (1998). Late Cenozoic tectonic evolution of the southern Chinese Tian Shan. *Tectonics*, *17*(1), 1–27. https://doi.org/10.1029/97TC03140

Zhao, G., Wang, Y., Huang, B., Dong, Y., Li, S., Zhang, G., & Yu, S. (2018). Geological reconstructions of the East Asian blocks: From the breakup of Rodinia to the assembly of pangea. *Earth-Science Reviews*, *186*, 262–286. https://doi.org/10.1016/j.earscirev.2018.10.003

Zhou, Y. N. (2025). Paleomagnetic data show a Qaidam-North China connection: The paradox of the last major Intra-Asian plate boundary [Dataset]. *figshare*. https://doi.org/10.6084/m9.figshare.28211645.v2

Zijderveld, J. (1967). AC demagnetization of rocks: Analysis of results. In *Methods in paleomagnetism DW Collinson, KM creer, SK runcorn* (pp. 254–286). Elsevier. https://doi.org/10.1016/B978-1-4832-2894-5.50049-5.11.

References From the Supporting Information

Hounslow, M. W., & Balabanov, Y. P. (2018). A geomagnetic polarity timescale for the Permian, calibrated to stage boundaries. *Geological Society, London, Special Publications*, *450*(1), 61–103. https://doi.org/10.1144/SP450.8